UAV-based Antenna Measurements: Scan Strategies

Fabio Paonessa[1], Giuseppe Virone[1], Pietro Bolli[2], Andrea M. Lingua[1,3]
[1] Istituto di Elettronica e di Ingegneria dell'Informazione e delle Telecomunicazioni (IEIIT), Consiglio Nazionale delle Ricerche (CNR), Torino, Italy, giuseppe.virone@ieiit.cnr.it
[2] Osservatorio Astrofisico di Arcetri (OAA), Istituto Nazionale di Astrofisica (INAF), Firenze, Italy
[3] Dipartimento di Ingegneria dell'Ambiente, del Territorio e delle Infrastrutture (DIATI), Politecnico di Torino, Torino, Italy

***Abstract*—In the recent years, the authors developed a system for the characterization of the radiation pattern of VHF and UHF antennas by means of a test-source mounted on a micro Unmanned Aerial Vehicle (UAV). So far, the adopted scan strategies typically consisted of two orthogonal straight paths at constant height from ground to obtain *E*- or *H*-plane cuts. In this paper, more complex scan strategies are presented to perform two-dimensional pattern measurements over planar and curved surfaces.**

***Index Terms*—antenna measurements, unmanned aerial vehicles, UAV.**

I. Introduction

In the recent years, UAV-mounted radio sources have been exploited by researchers to perform in-situ antenna pattern measurements [1]–[5]. In particular, the authors developed a system to characterize the radiation pattern of VHF and UHF ground-based antennas for radio astronomy observations (see Fig. 1). This UAV-based far-field test-source has been successfully used to characterize both single elements [6]–[8] and arrays [9] [10] in the frequency range from 45 MHz to 650 MHz.

The typical measurement strategy consists of a rectilinear constant-height flight trajectory lying in the *E*- or *H*-plane of the antenna radiation pattern (Fig. 2). Moreover, since the flying test source is linearly-polarized [11], co-/cross-polar measurements can be performed by setting the proper UAV orientation in the horizontal plane (yaw angle) [12]. The craft can also hover at the zenith of the Antenna Under Test (AUT) and rotate slowly around the vertical axis to investigate the AUT polarization properties [8].

Such linear/punctual scan strategies only provide partial information on the AUT radiation pattern. However, they are simple and reliable from the point of view of the flight dynamics and accuracy of execution. The corresponding AUT pattern data are obtained by post-processing the received power at the AUT port according to [13].

It should be noted that, in a rectilinear flight, the distance between the test-source and the AUT becomes larger for increasing values of zenith angle (scan angle from zenith). The increasing path loss with respect to the zenith angle will slightly affect the required receiver dynamic range. Furthermore, the long flying distance required to reach high zenith angles generally leads to a quite long (non-optimum) flight duration, which already represents a limiting factor for battery-powered UAVs.

Exploiting the recent developments of the UAV technology, more complex flight strategies with variable height can be planned in order to both optimize the above mentioned parameters and obtain information over a planar or curved surface rather than linear cuts. In this case, the purpose is to perform several scans with a time-effective strategy and combine the data, obtaining a two-dimensional representation of the AUT pattern.

The next section presents some of the scan strategies recently employed by the authors to perform two-dimensional pattern measurements. Such examples of implemented flight trajectories were measured using the onboard GPS unit. The corresponding measured antenna patterns will be shown at the conference.

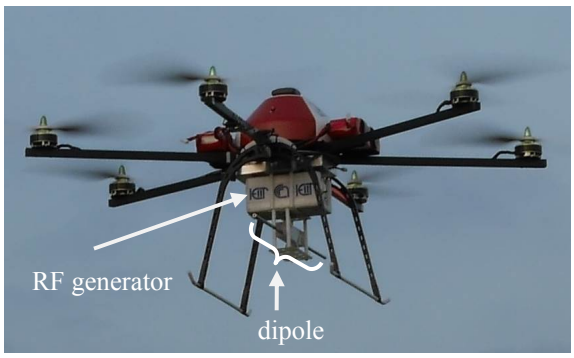

Fig. 1. The UAV-mounted radio source, which consists of an RF generator and a dipole antenna.

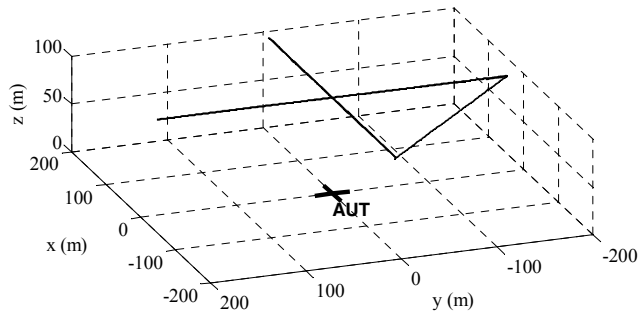

Fig. 2. Typical flight trajectory to obtain *E*- or *H*-plane cuts. The extension is ±180 m at 100 m height, i.e. ±60° of zenith angle variation. Take-off and landing paths not shown.

II. RASTER SCAN STRATEGIES

A. Cartesian raster

The Cartesian raster in Fig. 3a consists of several rectilinear parallel flight paths performed at a constant height and with constant UAV orientation. Such orientation is usually parallel or perpendicular to the direction of the segments, providing two orthogonal field components. However, it requires quite large power consumption and flight time because of the many veers the craft has to perform, reducing the average speed.

Such a flying strategy has already been used in the far-field of an array in order to map specific details of the radiation patterns such as the main beam. Moreover, it has also been used as a near-field scan strategy: the experimental case of Fig. 3a has been performed at 25 m height inside a square area with extension of ±20 m both along x and y, i.e. 39° of zenith angle extension. The spacing between adjacent paths is 0.75 m, which gives a total flight length of about 2400 m. As a first step, this strategy will be used to verify amplitude-only near-field simulation data. Further research work is being carried out in order to obtain the phase measurement as well. In this way, the far-field pattern could be derived from such a near-field distribution. This evolution would enable the characterization of very large installations for which the required far-field distance would prevent a small UAV to be exploited. The concept of UAVs as near-field positioners has already been reported in [14].

B. Radial raster

The radial raster shown in Fig. 3b develops on a planar surface. However, it can be implemented with curved segments as well. It consists of several rectilinear constant-height paths having radial direction with respect to the vertical axis. The UAV yaw angle is kept constant within a single segment, i.e. parallel or perpendicular to the radial direction. In this way, either the θ- or φ- component of the radiation pattern can be detected, respectively. It should be noted that additional post-processing is still required in order to obtain the two components of the AUT pattern from the measured data.

The flight efficiency, in terms of covered area vs. time, is higher than the Cartesian raster. However, the sampling density is higher close to the zenith and reduces as the distance increases. In the case of Fig. 3b, the flight height is 100 m and the circular area given by the flight envelope has a radius of 150 m, which corresponds to approximately 56° of zenith angle. The azimuthal angular pitch is 22.5° and the total flight length is 3400 m.

C. Azimuthal 3D raster

The azimuthal raster (Fig. 3c) consists of several circular concentric paths that are performed at different heights in order to maintain a constant distance from the AUT. This feature will lead to both a constant path loss and minimum flight duration. It should be noted that the azimuthal sampling density is more uniform with respect to the radial raster. Moreover, although the flight envelope is three-dimensional, a single circular path has a constant height, which provides high flight accuracy.

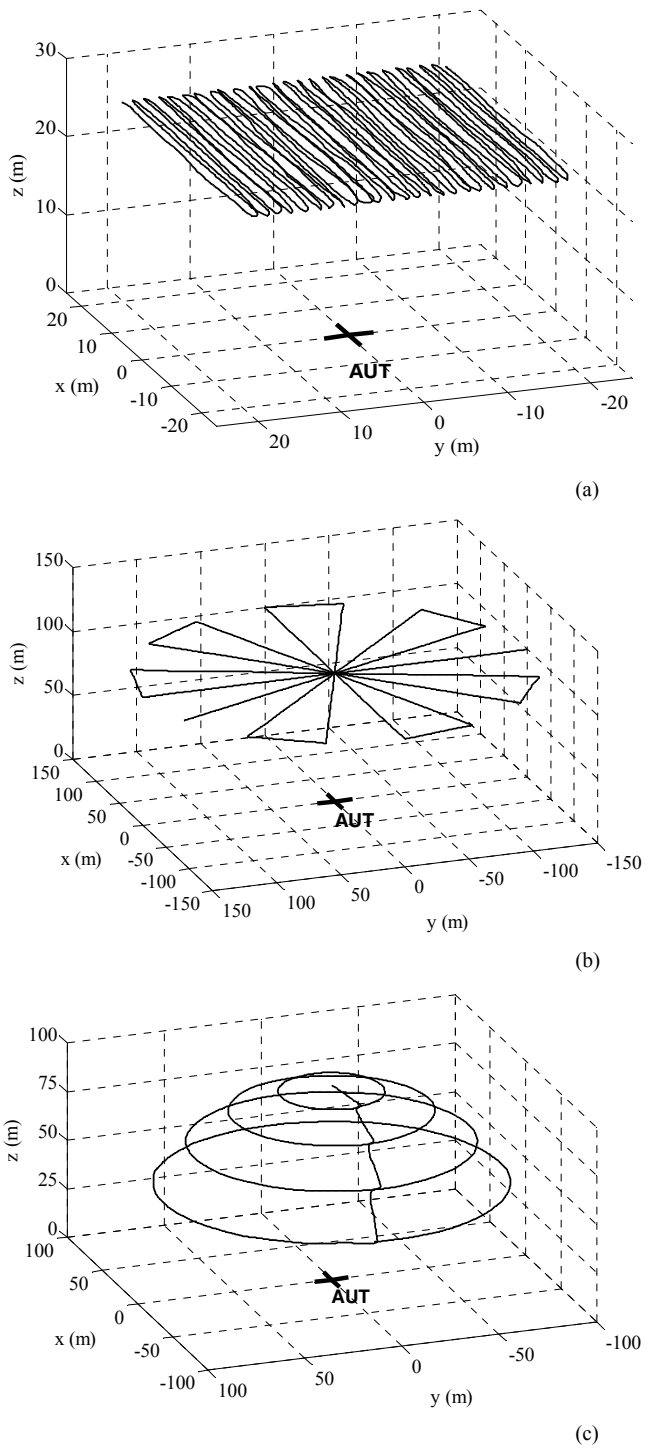

Fig. 3. Measured flight trajectories of (a) a Cartesian raster, (b) a radial raster and (c) an azimuthal 3D raster. Take-off and landing paths not shown.

Differently from [15], the UAV orientation (yaw) should be set as parallel (perpendicular) to the flight direction (speed

vector) in order to detect either the φ- (θ-) component. It should be noted that the UAV horizontal orientation continuously varies also within a single circular path. This behavior could be not straightforward to implement with some pilot platforms. Subsequent post-processing will be required in order to obtain the AUT pattern.

In the case of Fig. 3c, the distance between the AUT and the test-source is 100 m during the whole flight. The surface envelope extends to 60° of zenith angle with 15° steps and a total flight length of 1750 m.

III. CONCLUSION

Due to the limited accuracy of the onboard GPS-based navigation controller and the effects of external disturbances (e.g. wind), the real flight trajectories can differ from the planned ones by a few meters. Such a discrepancy is usually slowly fluctuating (see path of Fig. 3a).

The GPS accuracy is not sufficient to compute the AUT pattern with the desired level of accuracy. For this reason, the flight trajectory is also measured with an additional Differential Global Navigation Satellite System (DGNSS), which provides centimeter-level accuracy. The discrepancy between the paths measured with the GPS and the DGNSS is generally consistent with a slow-varying error of few meters rather than a random variation.

REFERENCES

[1] G. Virone, et al., "Antenna Pattern Verification System Based on a Micro Unmanned Aerial Vehicle (UAV)," IEEE Antennas and Wireless Propagation Letters, vol.13, pp. 169-172, Jan. 2014.

[2] C. Chang, et al., "Beam calibration of radio telescopes with drones," Publications of the Astronomical Society of the Pacific, vol. 127, no. 957, 2015.

[3] F. Üstüner, et al., "Antenna radiation pattern measurement using an unmanned aerial vehicle (UAV)," General Assembly and Scientific Symposium (URSI GASS), 2014 XXXIth URSI, Beijing, 2014, pp. 1-4.

[4] L. Washburn, E. Romero, C. Johnson, B. Emery, C. Gotschalk, "New applications for autonomous aerial vehicles (drones) in coastal oceanographic research", Ocean Sciences Meeting 21-26 Febraury 2016, New Orleans, Louisiana, USA.

[5] A. Nelles, et al, "Calibrating the absolute amplitude scale for air showers measured at LOFAR", JINST 10 (2015) no.11, P11005 arXiv:1507.08932.

[6] F. Paonessa, et al., "UAV-based pattern measurement of the SKALA," in IEEE Antennas and Propagation Society International Symposium (AP-S/URSI), Vancouver, Canada, July 19-25 2015.

[7] F. Paonessa, et al., "VHF/UHF Antenna Pattern Measurement with Unmanned Aerial Vehicles," in IEEE International Workshop on Metrology for Aerospace (MetroAeroSpace), Florence, Italy, June 22-23 2016.

[8] P. Bolli, et al., "Antenna pattern characterization of the low-frequency receptor of LOFAR by means of an UAV-mounted artificial test source," in SPIE Ground-based and Airborne Telescopes VI, Edinburgh, Scotland, United Kingdom, June 26 – July 1 2016.

[9] P. Bolli, et al., "From MAD to SAD: the Italian experience for the Low Frequency Aperture Array of SKA1-LOW", Radio Science, vol. 51, issue 3, pp. 160–175, Mar. 2016.

[10] G. Pupillo, et al., "Medicina Array Demonstrator: calibration and radiation pattern characterization using a UAV-mounted radio-frequency source," Experimental Astronomy, vol. 39, issue 2, pp. 405-421, June 2015.

[11] G. Virone, et al., "Antenna Pattern Measurement with UAVs: Modeling of the Test Source," European Conference on Antennas and Propagation (EuCAP), Davos, Switzerland, Apr. 11-15 2016.

[12] F. Paonessa, et al., "Antenna Pattern Measurement with UAVs: Cross Polarization Performance," 36th ESA Antenna Workshop on Antennas and RF Systems for Space Science, Oct. 6-9 2015, Noordwijk, the Netherlands.

[13] G. Virone, et al., "Antenna pattern measurements with a flying far-field source (hexacopter)," in IEEE International Conference on Antenna Measurements and Applications (CAMA), Antibes Juan-les-Pins, France, Nov. 16-19 2014.

[14] T. Fritzel, H.-J. Steiner, J. Habersack, H. Schippers, J.-G. Ferrante, "Antenna Pattern Measurements of Full-Size Air Vehicles with an Airborne Near-field Test Facility (ANTF)" European Test & Telemetry Conference, ETTC 2005, Toulouse, France.

[15] D. Jacobs, "Report on ECHO measurements of ORBCOMM dipoles in Green Bank," Aug. 28 2015.